Received: 7 October 2022 | Accepted: 2 December 2022

DOI: 10.1002/pamm.202200148

Electrostatic Body Forces and their Implications for Cracks

Alexander Schlosser[1,*] and **Andreas Ricoeur**[1]

[1] University of Kassel, Institute of Mechanics, Moenchebergstr. 7, 34125 Kassel, Germany

A Griffith-type crack in a dielectric solid under electromechanical loading is investigated by numerically solving the combined boundary value problem. The focus is on the contribution of electrostatically induced body forces, coming along with the still controversially discussed Maxwell stress tensor, to the crack tip loading. A $1/r$-singularity of compressive stress is found to evolve at the crack tip, however, just being dominant over the mechanically induced $1/\sqrt{r}$-behavior within a very small region.

1 Introduction

Electrical loads do not only cause stresses in piezoelectrics and ferroelectrics. Also in dielectrics without piezoelectric coupling properties they cause so-called Maxwell stresses, which can be of interest in the context of fracture mechanics. One part of these Maxwell stresses, which occurs on interfaces, e. g. crack faces, has already been considered in some publications and has a relevant influence on the loading of the crack tip under certain conditions, depending on the ratios of dielectric constants as well as electric and mechanical loading. Another part of the Maxwell stresses, which occurs as a body force, has been neglected in fracture mechanics so far. The aim of the work at hand is therefore to investigate the influence of these body forces by incorporating them into a selected problem of linear elastic fracture mechanics with static electromechanical loadings.

2 Theoretical framework

As mentioned above Maxwell stresses act in two ways. On the one hand they occur as surface tractions t_i^{em} at every bi-material interface in dielectric bodies. This stress vector is linked to the Maxwell stress tensor T_{ij} via

$$t_i^{\mathrm{em}} = \left(T_{ij}^{\mathrm{interior}} - T_{ij}^{\mathrm{exterior}}\right) n_j^{\mathrm{exterior}}. \tag{1}$$

The superscripts denote the two sides of the interface and may, e. g., denote the interior and exterior, respectively, of a crack slit. On the other hand, they occur everywhere in dielectric bodies as body forces which are also derived from the Maxwell stress tensor according to

$$f_i^{\mathrm{em}} = T_{ij,j}. \tag{2}$$

While there is widespread agreement on the definition of the Maxwell stress tensor in vacuum, its formulation in matter is part of a century-long controversy [1]. Some most famous contributions to this controversy are collected in Tab. 1. For the

Minkowski [2]	Abraham [3]	Einstein and Laub [4]
$T_{ij}^{\mathrm{M}} = E_i D_j - \frac{1}{2}(E_k D_k)\delta_{ij}$	$T_{ij}^{\mathrm{A}} = \mathrm{sym}(T_{ij}^{\mathrm{M}})$	$T_{ij}^{\mathrm{EL}} = E_i D_j - \frac{1}{2}(\kappa_0 E_k E_k)\delta_{ij}$

Table 1: Prominent definitions of the electrostatic Maxwell stress tensor in matter.

following investigations the definition of Einstein and Laub is used, which leads to the body force

$$f_i^{\mathrm{em}} = (\kappa_{\mathrm{bulk}} - \kappa_0) E_j E_{j,i}, \tag{3}$$

where κ_{bulk} is the permittivity of the material and κ_0 is the one of vacuum. To investigate the effect of these body forces on cracks numerically, the model depicted in Fig. 1 is used in combination with the FEM package FEniCS. It is loaded purely electrically via the arbitrary surface charge densities $\overline{\omega}^{\mathrm{s}} = -\overline{\omega}^{\mathrm{n}} = D_2^{\infty}$ at the upper and lower boundaries and the crack is assumed impermeable for electric fields ($\overline{\omega}^{\mathrm{crack}} = 0$). The latter condition leads to traction free crack faces since all components of t_i^{em} in Eq. 1 vanish. The material of the plate is assumed to be isotropic and dielectric with Young's modulus $E = 210\,\mathrm{GPa}$, Poisson's ratio $\nu = 0.3$ (the results will be independent of E and ν) and an electric permittivity $\kappa_{\mathrm{bulk}} = 10\kappa_0$. In this case the electrical problem, given in weak formulation according to

* Corresponding author: e-mail alexander.schlosser@uni-kassel.de, phone +49 561 804 3606

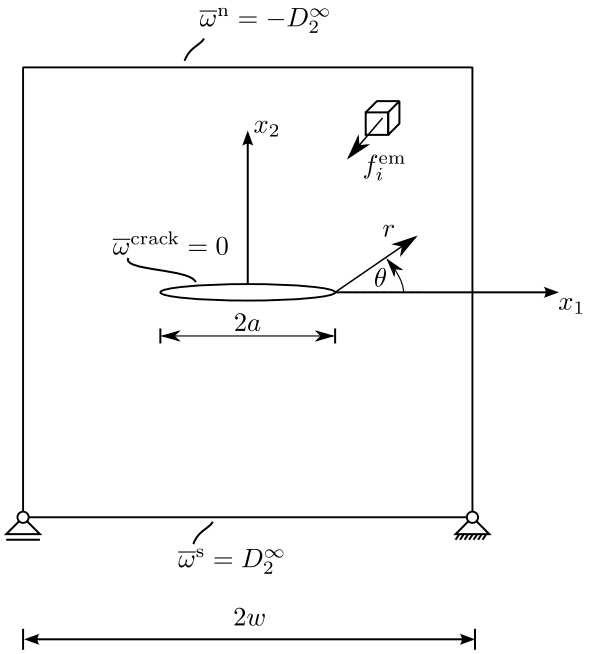

Fig. 1: Center crack in a square plate ($w/a = 10$) with electrical boundary conditions $\overline{\omega}^{\mathrm{s}}$, $\overline{\omega}^{\mathrm{n}}$ and $\overline{\omega}^{\mathrm{crack}}$.

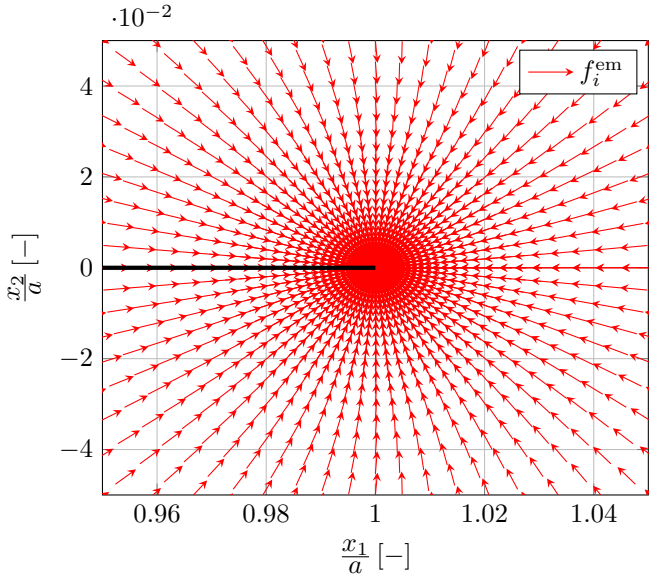

Fig. 2: Unit vectors of body forces in the vicinity of the crack tip calculated via Eq. 3. The cartesian coordinate system (x_1, x_2) is located in the center of the square plate, see Fig. 1, and the crack is marked as black line.

$$\int_V \kappa_{\mathrm{bulk}} E_j \delta E_j \mathrm{d}V - \int_A \overline{\omega} \delta\varphi \mathrm{d}A = 0, \tag{4}$$

where φ is the electric potential, and the mechanical weak formulation

$$\int_V \sigma_{kl} \delta\epsilon_{kl} - f_i^{\mathrm{em}} \delta u_i \mathrm{d}V = 0 \tag{5}$$

are coupled only unilaterally, so that the electrical one can be solved independently resulting in an electric field. Based on the latter, the body force vector f_i^{em} is then calculated via Eq. 3 at every node of the FEM mesh and finally plugged into Eq. 5 which is subsequently solved. The unit vectors of the body force, which where calculated with this procedure, are depicted in the vicinity of the crack tip in Fig. 2.

3 Results

For assessments in the context of fracture mechanics the stresses σ_{12} and σ_{22} at the ligament near the crack tip ($r/a \ll 1, \theta = 0$) are of particular interest and are thus depicted in Fig. 3. While there are no shear stresses σ_{12} of relevant magnitude, there

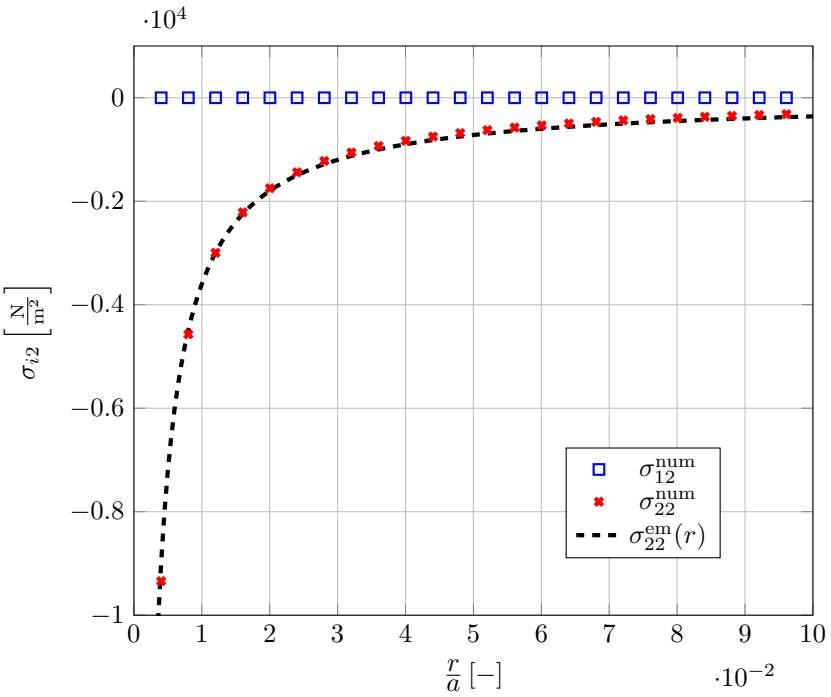

Fig. 3: Numerically calculated and via Eq. 6 approximated stresses on the ligament.

seems (can not be proven rigorously on the basis of a numerical solution) to be a singular compressive stress at $r \to 0$ due to the electric loading. By means of parameter studies and dimensional analysis it could be found that this compressive stress is well approximated by

$$\sigma_{22}^{\mathrm{em}}(r, \theta = 0) = \underbrace{-\frac{a}{2}(D_2^\infty)^2\Big(\frac{1}{\kappa_{\mathrm{bulk}}} - \frac{\kappa_0}{\kappa_{\mathrm{bulk}}^2}\Big)}_{L} r^{-1} \tag{6}$$

in the vicinity of the crack tip (see black dashed line in Fig. 3). The approximation is independent of the sign and proportional to the square of the electric loading D_2^∞. The most peculiar property, however, is its $1/r$-singularity, which surpasses the classical $1/\sqrt{r}$-singularity of mechanically induced stresses in linear elastic fracture mechanics. Consequently, the application of classical stress intensity factors as crack tip loading quantities is obsolete. In order to assess the quantitative influence of the electrically induced stresses, a study with electromechanical loading is performed in the following. If the above described crack is additionally loaded with a tensile stress σ_{22}^∞, the relevant stress on the ligament becomes

$$\sigma_{22}(r) = \sigma_{22}^{\mathrm{mech}}(r) + \sigma_{22}^{\mathrm{em}}(r) = \frac{K_I}{\sqrt{2\pi r}} + \frac{L}{r} \tag{7}$$

by superposition. The first term is the classical $1/\sqrt{r}$ -singularity with the stress intensity factor $K_I = \sigma_{22}^\infty\sqrt{\pi a}$ and the second term is the approximation from Eq. 6 where all constant terms are collected in L. The opposing signs of L and K_I together with the different types of singularities leads to a stress distribution on the ligament which has two characteristic points. The first one is a maximal stress

$$\sigma^{\max} = -\frac{1}{4\pi}\frac{K_I^2}{L} = \Big(\frac{\sigma_{22}^\infty}{D_2^\infty}\Big)^2 \frac{1}{4\Big(\frac{1}{\kappa_{\mathrm{bulk}}} - \frac{\kappa_0}{\kappa_{\mathrm{bulk}}^2}\Big)} \tag{8}$$

at the distance

$$r^{\max} = 8\pi\Big(\frac{L}{K_I}\Big)^2 = 8\frac{\big(D_2^\infty\big)^4}{\big(\sigma_{22}^\infty\big)^2}\Big(\frac{1}{\kappa_{\mathrm{bulk}}} - \frac{\kappa_0}{\kappa_{\mathrm{bulk}}^2}\Big)^2 a \tag{9}$$

from the crack tip which is indicated by a triangle in Fig. 4. The second characteristic point is a root of Eq. 7 at

$$r^{\mathrm{com}} = \frac{1}{4} r^{\max} \tag{10}$$

below which the stress is always compressive, if there is an electric load. To get an estimate for the mentioned radii, Fig. 5

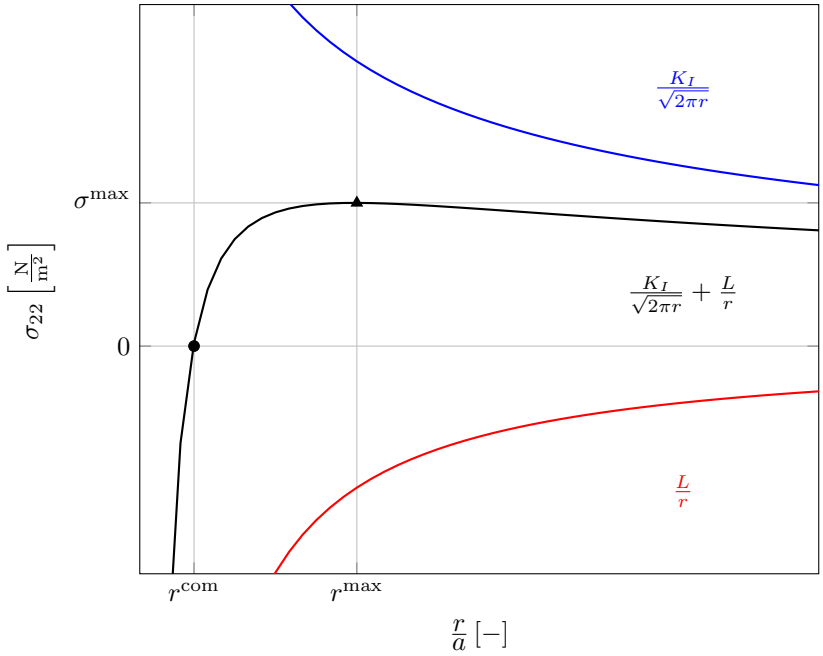

Fig. 4: Mechanically induced (blue), electrically induced (red) and combined (black) stresses in the vicinity of a crack tip.

shows the ratio of the electrically and mechanically induced stress for various electric loads $E_2^\infty = D_2^\infty/\kappa_{\mathrm{bulk}}$ in dependence of the radius. As largest electric load $E_2^\infty = 10^6\,\mathrm{V/m}$ is chosen, since most dielectric materials break down electrically at this load. In order to provide an upper limit of the effect of the body forces, a comparatively small mechanical load $K_I = 1\,\mathrm{MPa}\sqrt{\mathrm{m}}$, a typical permittivity of dielectrics $\kappa_{\mathrm{bulk}} = 10\kappa_0$ and a large crack length of $a = 100\,\mathrm{mm}$ are chosen. Additionally, the typical radius of atoms $r_{\mathrm{atom}} \approx 10^{-10}\,\mathrm{m}$ is indicated by a vertical dashed line for the sake of comparison. Since the maximum radius of compressive stress r^{comp} is coming along with a ratio $\sigma_{22}^{\mathrm{em}}/\sigma_{22}^{\mathrm{mech}} = -1$, marked as circles in Fig. 5, it becomes clear that the radii where the electrostatic body forces have a significant influence are negligibly small. Since larger electric fields are impossible for most materials and smaller mechanical loads are irrelevant in terms of fracture mechanics, these radii could only increase in the case of even larger crack lengths, since they are proportional to a (compare Eq. 9). A similar consideration can be made for the maximal stress from Eq. 8, which is included as triangles in Fig. 5 and plotted double-logarithmically vs. the electric load in Fig. 6. Even if the maximal electric load is applied, there is still a high maximal tensile stress of about $10^4\,\mathrm{MPa}$. Furthermore, per every order of magnitude the electric load is decreased, the maximal stress increases by two orders of magnitude, independently of the crack length a, see Eq. 8. So there is always a large tensile stress concentration in the vicinity of the crack tip and the distance $r^{\max}$, where the maximal stress occurs, is smaller than an atom radius.

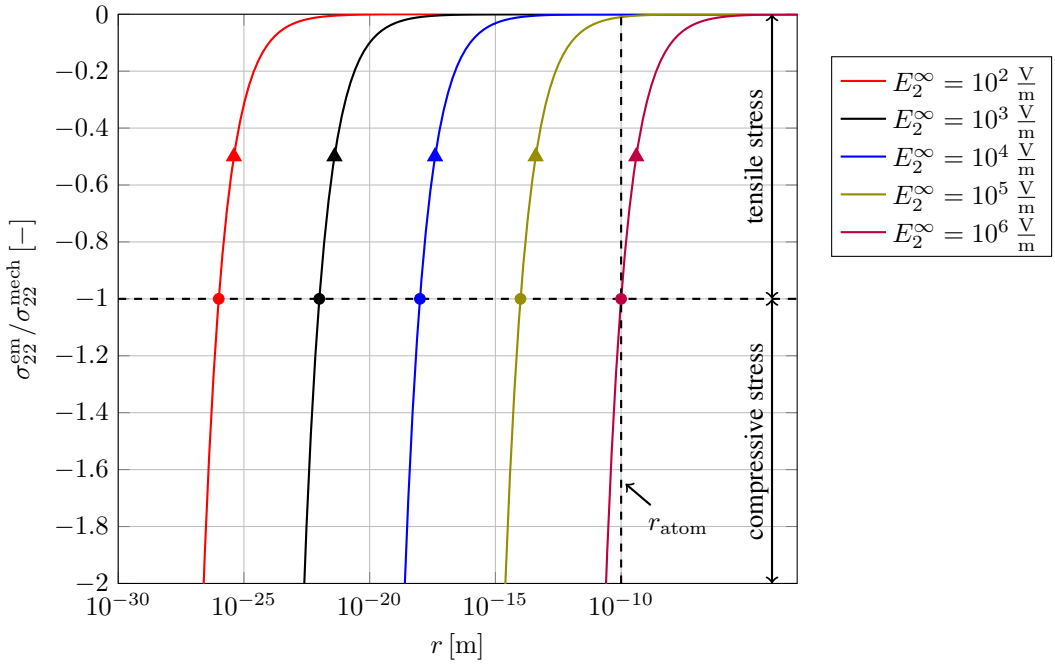

Fig. 5: Ratio of electrically and mechanically induced stresses in the vicinity of the crack tip for a range of electric loads and a constant mechanical load corresponding to $K_I = 1\,\mathrm{MPa}\sqrt{\mathrm{m}}$. The radii of maximal stress according to Eq. 9 are marked with triangles and the radii of compressive stress from Eq. 10 are marked as circles. The electric permittivity is $\kappa_{\mathrm{bulk}} = 10\kappa_0$ and the crack length is $a = 100\,\mathrm{mm}$.

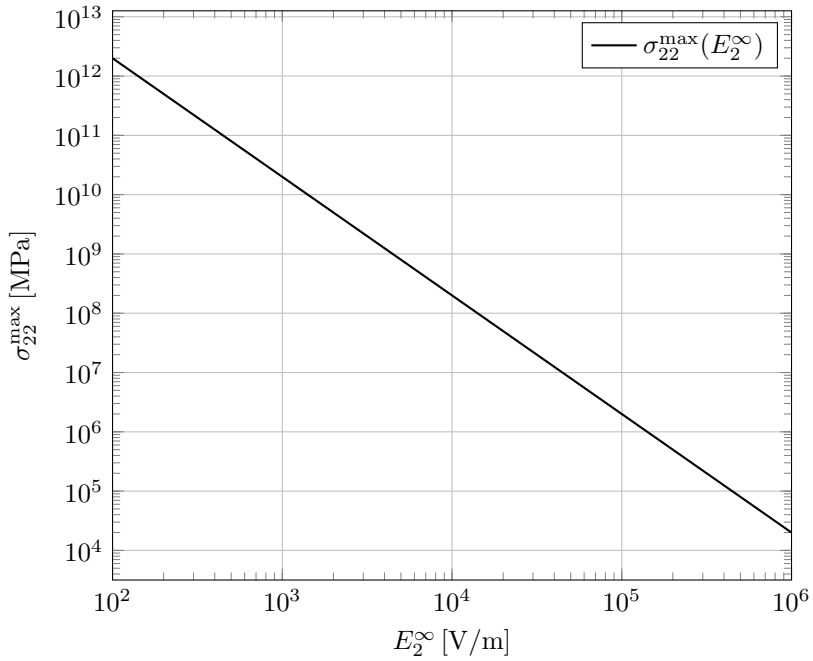

Fig. 6: Maximum stress from Eq. 8 vs. electric load for a constant mechanical load corresponding to $K_I = 1\,\mathrm{MPa}\sqrt{\mathrm{m}}$. The electric permittivity is $\kappa_{\mathrm{bulk}} = 10\kappa_0$ and the crack length is $a = 100\,\mathrm{mm}$.

4 Conclusion

A $1/r$-singularity due to electrostatic body forces could be identified by numerical solution of an electrostatic-elastic crack problem. Being superimposed with a classical $1/\sqrt{r}$-singularity from mechanical loading, compressive stress prevails in a region at the crack tip being below an atomic radius. The stresses are further dominated by the $1/\sqrt{r}$-behavior at distances of the same order of magnitude away from the crack tip. Nevertheless, compressive stress prevails at the crack tip, indicating a crack closure in spite of tensile mechanical loading, however, the model being based on the continuum hypothesis, is violated on the nano scale. It should be noted at this point that the radius r^{com} is expected to be much larger in the case

of piezoelectricity, where the dielectric permittivity exceeds the value assumed here by two orders of magnitude. Studies employing other common formulations for the Maxwell stress tensor are in progress, indicating qualitatively different impacts on crack tip stress fields.

Acknowledgements Open access funding enabled and organized by Projekt DEAL.

References

[1] Corrêa, Raul and Saldanha, Pablo L.(2020) Hidden momentum in continuous media and the Abraham-Minkowski debate. Physical Review A , 102(6).

[2] Minkowski, H. (1910) Die Grundgleichungen für die elektromagnetischen Vorgänge in bewegten Körpern Mathematische Annalen, 68(4), 472-525.

[3] Abraham, M. (1909) Zur elektrodynamik bewegter Körper. Rendiconti del Circolo Matematico di Palermo (1884-1940), 28(1), 1-28.

[4] Einstein, A. and Laub, J. (1908) Über die im elektromagnetischen Felde auf ruhende Körper ausgeübten ponderomotorischen Kräfte. Annalen der Physik , 331(8), 541-550.

